Journal of Colloid and Interface Science 363 (2011) 122–128

Contents lists available at ScienceDirect

Journal of Colloid and Interface Science

www.elsevier.com/locate/jcis

Enhancement of β-crystalline phase of poly(vinylidene fluoride) in the presence of hyperbranched copolymer wrapped multiwalled carbon nanotubes

Linghao He [a], Jing Sun [a], Xiuxin Wang [b], Lu Yao [a], Jialong Li [a], Rui Song [a,b,*], Yongmei Hao [b], Yujian He [b,*], Wei Huang [c]

[a] *State Key Lab of Surface and Interface Sciences, Zhengzhou University of Light Industry, Zhengzhou 450005, China*
[b] *College of Chemistry and Chemical Engineering, Graduate University of Chinese Academy of Sciences, Beijing 100049, China*
[c] *Laboratory of Advanced Polymer Materials, Institute of Chemistry, Chinese Academy of Sciences, Beijing 100080, China*

ARTICLE INFO

Article history:
Received 6 May 2011
Accepted 14 July 2011
Available online 22 July 2011

Keywords:
Poly(vinylidene fluoride)
Multiwalled carbon nanotubes
Crystallization
Hyperbranched copolymer

ABSTRACT

Many efforts have been performed on the poly(vinylidene fluoride), PVDF, due to its piezoelectric, pyroelectric and ferroelectric potentials. In this regard, how to fabricate the PVDF with high content of β-phase, which is also the direct contribution to PVDF's prominent property, becomes a critical issue. In this study, starting with the α-phase dominated sample, the PVDF with extremely high content of β-crystalline phase was obtained by the incorporation of multiwalled carbon nanotubes (MWCNTs) modified by hyperbranched copolymers (HBCs). We proved that, *via* XRD, DSC as well as the structural characterizations from the polarized optical microscopy and transmission electron microscopy (TEM), the success of this strategy was ascribed to the enhanced dispersibility and stability of MWCNTs endowed by the HBCs, which significantly favors the formation of the β-crystalline phase of PVDF.

1. Introduction

Over the last decade, poly(vinylidene difluoride) (PVDF) has attracted much research interest owing to its potential applications as piezoelectric, pyroelectric and ferroelectric materials. As well investigated, this potential was directly rendered by the specific distribution of crystal phases. Being one of the polymers with copious polymorphs, PVDF is able to crystallize in five different forms, which involve three different chain conformations, namely, *TTTT* for β phase, *TGTG′* for α and δ phases, *TTTGTTTG′* for γ and ε phases [1].

Although each PVDF polymer chain has an effective molecular dipole moment, while in molecular scale, only the β and γ phases have dipole moment in the crystalline state. In contrast, the PVDF chains in the α phase stack with their respective polarizations in alternating directions, resulting in a paraelectric behavior, therefore it is nonpolar. The all-trans β phase is the most polar with the polymer chains stacking with their respective polarizations aligned in the same direction. As a consequence, enhancement of the content of the polar β phases and simultaneous suppression of the nonpolar α phase in PVDF material is of great importance for its applications. To this end, many efforts have been performed on how to acquire pure or high content β phase. As reported, the β phase could be formed by high-pressure quenching from a melt or by casting from a strongly polar solvent, such as DMF or DMAc [2–4]. It can be also transformed from β phase by uniaxial or biaxial drawing [5,6].

Besides, two protocols are more frequently used for this aim. One is the incorporation of layered silicate (often referred as nanoclay) [7–13] or chemically-modified carbon nanotubes [14,15] into PVDF. The related results imply that the existence of ion–dipole interaction between negatively charged clay and positive CH_2 dipoles of PVDF results in the preferential formation of the β phase. Apart from these additives, oxidic spinnel Ni–Zn ferrite nanoparticles(NPs) [16,17] or $CoFe_2O_4$, Ni Fe_2O_4 NPs [18] had been added into the PVDF matrix. As another alternative, electrospinning, which involves the uniaxial stretching of a viscous polymer solution or melt in an electric field due to the electrostatic repulsions between surface charges along the jet, is a novel and effective technique to form the β phase of PVDF nanofiber [19–21].

Nowadays, minimization and high efficiency become a prerequisite in many application fields, such as sensor, information storage, etc. To meet this end, special attention has been paid for the preparation of the nanoscale thin films of PVDF containing high content of β-phase. The methods based on evaporative deposition [22], low-pressure chemical vapor polymerization [23], electrospray technique [24], and spin coating based thin film fabrication [25,26] have been investigated.

Meanwhile, hyperbranched polymers (HBCs) have good solubility, lower melt viscosity, and extremely high density of functional groups at the surface compared with the linear analogs, and there-

---

* Corresponding authors. Address: College of Chemistry and Chemical Engineering, Graduate University of Chinese Academy of Sciences, Beijing 100049, China. Fax: +86 10 88256092 (R. Song).
E-mail address: rsong@gucas.ac.cn (R. Song).

0021-9797/$ - see front matter © 2011 Elsevier Inc. All rights reserved.
doi:10.1016/j.jcis.2011.07.042

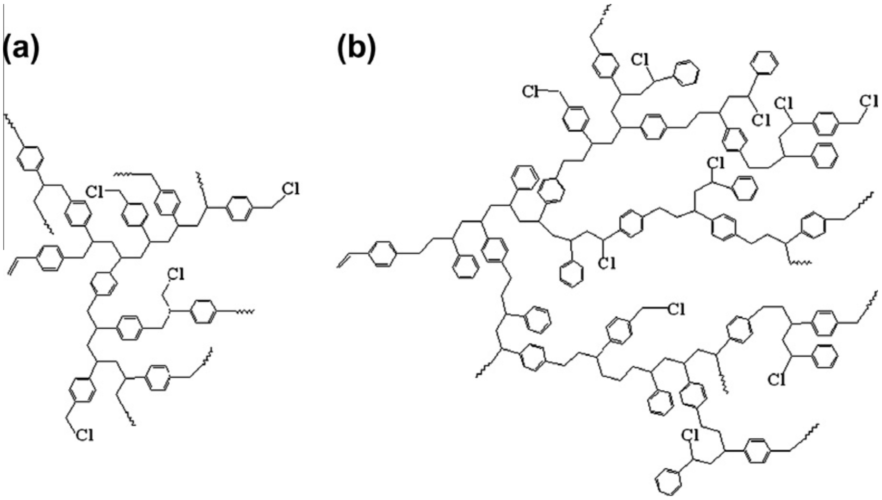

Fig. 1. Chemical structure formulas and abbreviations of hyperbranched copolymers used in this study. Hyperbranched p-chloromethylstyrene (a) and hyperbranched polystyrene copolymer (b).

fore increase the solubility of multiwalled carbon nanotubes (MWCNTs) or nanoparticles, such as Ag [27], and the stability of dispersion system. Herein, with the addition of MWCNTs which modified by four different HBCs (Fig. 1), we prepared stable, flexible PVDF nanofilms with relatively higher β phase content.

2. Experimental

2.1. Materials

Analytical grade dimethylformamide (DMF), sulfuric acid, nitric acid, from Regent Comp., Beijing, were used as received without further purification. The MWCNTs were purchased from Aldrich. They were first functionalized by refluxing in sulfuric acid and nitric acid mixture (3:1 = V/V) at 120 °C for 3 h, to give surface carboxyl groups at the defect sites of the outer graphene layer of the nanotubes and to remove residual metal-catalyst impurities [28]. Poly(vinylidene fluoride) ($M_n = 300{,}000$) with MFI (melt flow index) of 15 g/10 min was obtained from Wuxi Fluorine ST Co., China.

The HBCs used here were kindly supplied by Prof. L.Y. Zhang, GUCAS, the details about the synthesis could be found somewhere [29]. Some parameters of these HBCs were given in Table 1. It should be noted that the main difference between these four HBCs is the mole ratio between the styrene (St) and p-chloromethyl styrene (CMS), which leads to minor difference in their structures.

2.2. Sample preparation

Solution coagulation was utilized to prepare the PVDF nanocomposites. All films, containing PVDF and MWCNTs, as well as the pure PVDF were prepared by the solvent casting method (the detail could be found in the experimental part in the Supplementary information). Firstly, purified MWCNTs (0.9 mg) and HBC-1 (0.3 mg), were dispersed in DMF (15 ml), respectively, and the mixtures were sonicated at room temperature for 1 h. Meanwhile, PVDF (0.3 g) was dissolved in DMF (15 ml). Then, the above solutions were blended and then sonicated for an additional 3 h at room temperature (Fig. 2). Finally, this uniform mixture was poured into a standard glass Petri dish prior to drying in the 120 °C oven for 18 h to evaporate residual solvent and get equilibrium weight. This film (S3) was peeled off of the substrates for subsequent measurements. In a similar way, a series of HBCs (including HBC-2, HBC-3, HBC-4) wrapped CNTs/PVDF composites films were prepared, i.e. S4, S5 and S6, respectively. Thus, these films have the same mass ratio of 1:3:1000 = HBC: CNTs: PVDF. As the control experiment, neat PVDF films were prepared under the same conditions. Detail about the samples, including the neat PVDF (S1), the CNTs-containing PVDF (S2) and the PVDF comprising the HBCs modified-CNTs could be found in Table S1 in Supplementary information.

2.3. Characterization

X-ray powder patterns were recorded on a D8 Advance, Bruker diffractometer in reflection mode, using copper-radiation, Cu Kα_1 radiation ($\lambda = 0.15418$ nm) operated at 40 kV and 30 mA. All samples were measured with a θ–2θ configuration with a step size of 0.02°. Optical images were observed by a polarized optical microscopy (POM, E600POL, Nikon). The FT-IR spectra was collected in the attenuated total reflection (ATR) mode with IR Tensor 27, Bruker Corp., DSC measurements of films (sample weight: ca. 3 mg) were performed on a TA Q100 DSC system, over a temperature range from 20 to 200 °C at the heating/cooling rates of 10 °C/min and a N_2 flow of 50 mL/min. The morphologies of the films

Table 1
Structure parameters of the HBCs.

Hyperbranched polymers	St (mol.%)[a]	CMS (mol.%)[b]	M_n (KDa)[c]	M_w (KDa)[c]	M_w/M_n[c]	2°-BCl/1°-BCl[d]
HBC-1 (homepolymer)	0	100	6.9	27.3	3.95	0.30
HBC-2	30	70	7.4	35.1	4.74	0.28
HBC-3	50	50	6.3	18.6	2.96	0.25
HBC-4	70	30	6.9	21.8	3.13	0.13

[a] Content of styrene in total monomers.
[b] Content of p-chloromethyl styrene in total monomers.
[c] Determined by GPC.
[d] Determined by ^{1}H NMR.

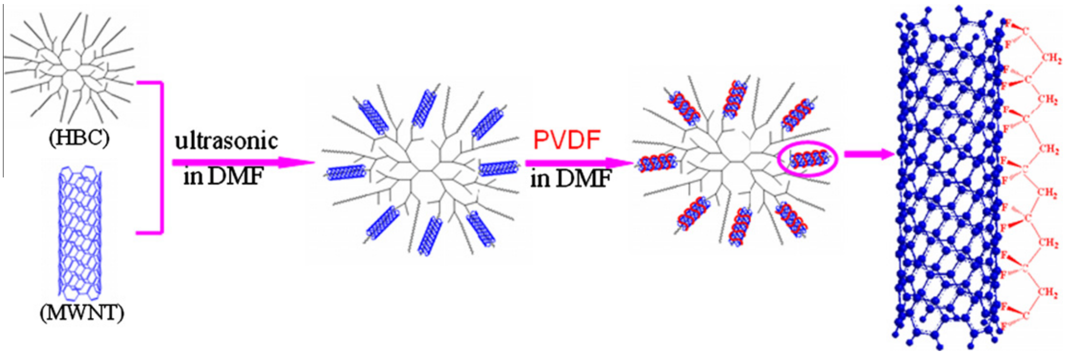

Fig. 2. Schematic diagram of the procedure used to prepare the PVDF-based hybrids comprising of the MWCNTs and MWCNTs modified by hyperbranched copolymer (HBCs).

were visualized by scanning electron microscopy (SEM) on a Hitachi S-4800 scanning electron microscopy at room temperature. Transmission electron microscopy (TEM) was carried out on a JEOL JEM 2100.

3. Results and discussions

To reveal the crystal phase in the hybrid films, X-ray diffraction experiments are preformed and the results are given in Fig. 3. The neat PVDF sample displays three peaks at $2\theta = 18.0 \pm 0.2°$ and $26.5 \pm 0.1°$, corresponding to the (1 0 0), (0 2 0) and (1 1 0) reflections of α phase, respectively [30]. Whereas, the peak appears at $2\theta = 20.2 \pm 0.2°$ corresponding to the (1 1 0) and (2 0 0) β planes, implying the existence of the β-phase [30]. In addition, the γ form diffraction, which normally appears at 14.8°, is not detectable [31].

As contrast, the intensity of α-phase is much lower than that of β-phase, which lead to a serious overlap at $2\theta = 18.0 \pm 0.2°$ by the β-phase peak. To evaluate the relative quantity of the different phase in the PVDF and PVDF hybrids, the peak fitting step is processed *via* the area of the peaks [30], by which we can calculate the quantity ratio between α and β phase with the following equation 1:

$$F_1(\beta) = \frac{S_\beta}{S_\alpha + S_\beta} \tag{1}$$

where S_α, S_β are the integral area of α and β phase in XRD patterns after the peak-fitting of superposition of the α and β phase, respectively.

Upon the addition of MWCNTs, particularly the addition of HBCs–dispersed MWCNTs, the variation in the polymorph of the hybrid films will be found. And this aspect could be well visualized from the significant decrease in the 26.5° peak, the diffraction solely ascribed to the β phase. Based on the peak-fitting process, the β phase will increase gradually, as a sharp comparison with that of the neat PVDF, which has ca. 9% of β phase content ($F_1(\beta)$). While, in the case of S4, the $F_1(\beta)$ can reach to a maximum of ca. 65%, implying a β phase dominant hybrid.

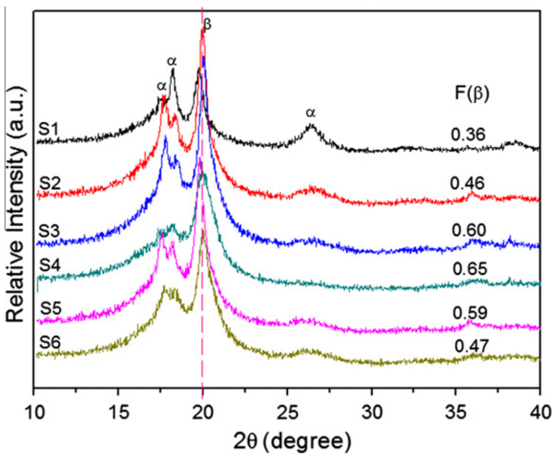

Fig. 3. XRD profiles of the pure PVDF (S1), hybrid films S2–S6.

A surprising consistence could be also verified from the differential scanning calorimetry (DSC) measurement. DSC heating and cooling curves were plotted in Fig. 4, and the corresponding data were summarized in Table S2 in Supplementary information. As clearly indicated in the first DSC heating curves in Fig. 4a, double-melting phenomena appear for all samples, including the neat PVDF, MWCNTs-incorporated PVDF and four hybrids comprising the PVDF and HBCs–dispersed MWCNTs. As a well documented phenomena, the exact assignment of the two melting peak is still in debate. As a more-accepted viewpoint, the two peaks located at 162 °C and 167 °C are related to melting of α and β phase, respectively [32,20]. In this context, it can be concluded that the neat PVDF is still α-phase dominated; upon addition of MWCNTs and HBCs–dispersed MWCNTs to the PVDF, the amount of α-phase decrease with a simultaneous increase of β phase. The exact content of β-phase ($F_2(\beta)$) can be calculated with the following equation:

$$F_2(\beta) = \frac{S_\beta}{S_\alpha + S_\beta} \tag{2}$$

where S_α and S_β are the area of α and β phase after the peak-fitting process of the DSC melting peaks, respectively, and the detail could be found in Fig. S1 in Supplementary information. As exhibited, the $F_2(\beta)$ display a maximum value of 57% in the case of S4. One thing noteworthy is, when the above samples are cooling down to room temperature and then subject to the second DSC heating scan, all the hybrids indicated a very similar shape as the neat PVDF (Fig. 4b). And from the melting point (~162 °C), it can be concluded that α-phase became the solely phase again in all samples, very similar to the single α-phase melting in the first DSC heating process of the montmorillonite clay based PVDF nanocomposites [33]. In addition, as clearly shown in the DSC cooling curves, the crystallizing points of the hybrid films (S2–S6) become lower than that of the neat PVDF (S1) (Fig. 4c). S4, particularly, has the lowest crystallizing point among the hybrid films. One possible reason behind this phenomenon is due to the relatively high thermal conductivity of MWCNTs comparing that of polymer matrix. Thus, even when small amount of MWCNTs is added into the hybrids, there would be a considerable improvement on the thermal conductivity of the composite [34,35]. More importantly, the more homogeneous dispersion of CNTs in the PVDF matrix would lead to a higher thermal conductivity of the hybrids, as previously reported for epoxy resin based composites with MWCNTs [36].

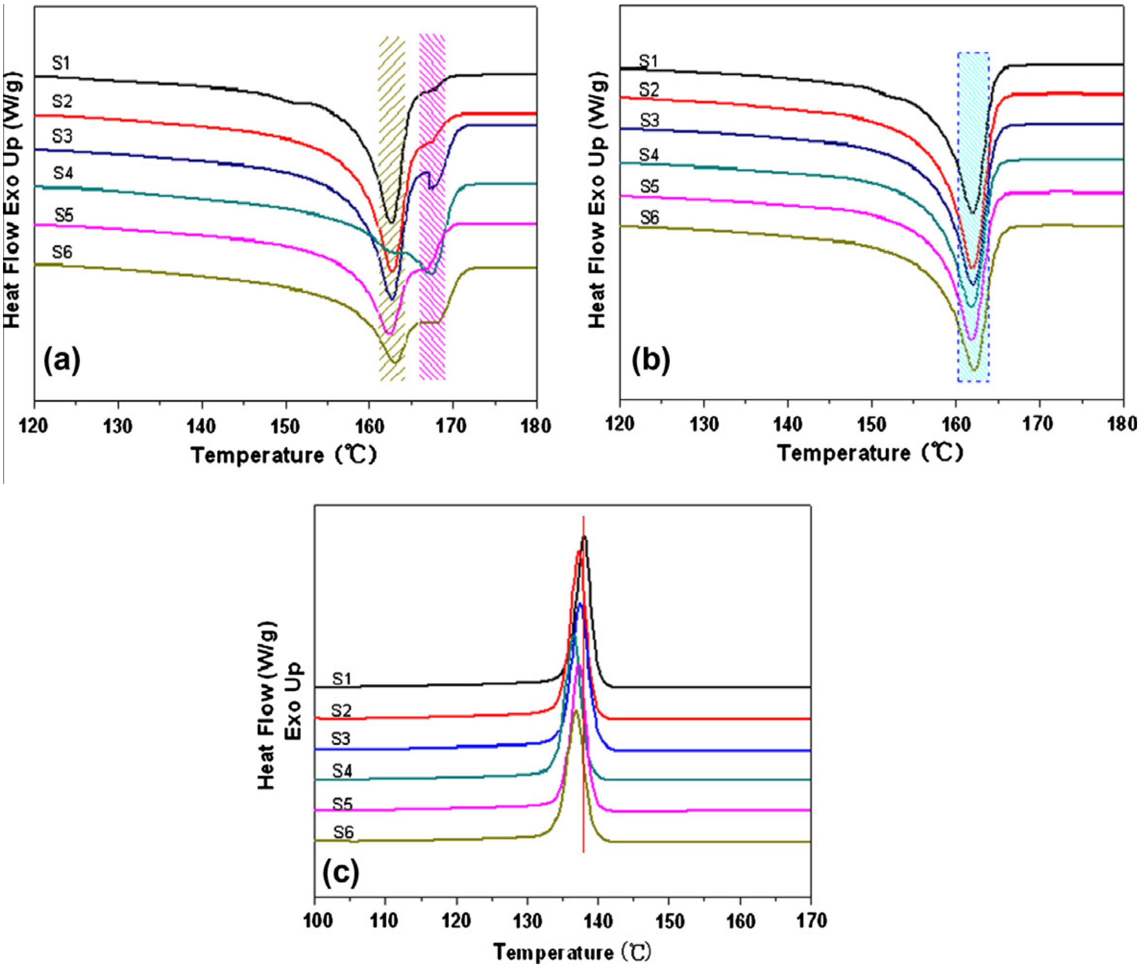

Fig. 4. DSC first-melting (a), second-melting (b) and crystallization (c) traces of the pure PVDF (S1), hybrid films S2–S6.

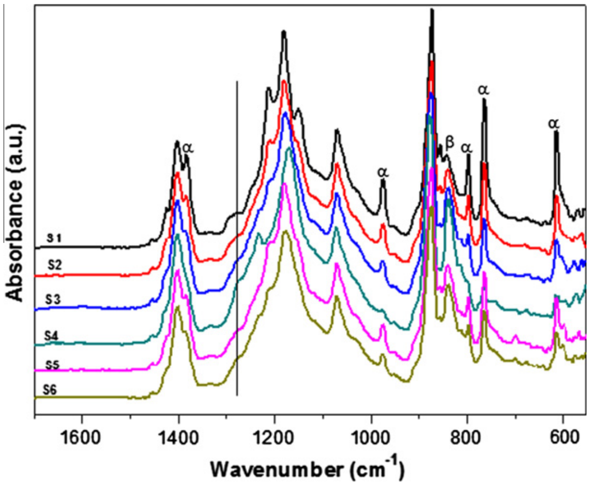

Fig. 5. FT-IR spectra of the pure PVDF (S1), hybrid films S2–S6.

FT-IR is another good technique for unambiguous identification of the crystal structure of PVDF. The bands at 532, 615, 764, 796, 855, 876, 976 and 1218 cm^{-1} are correspond to the *TGTG′* conformer of the α crystal phase; while the bands at 510, 840,1274 and 1284 cm^{-1} are related to the *TT* trans sequence (β phase), and the bands at 812 and 1234 cm^{-1} are assigned to γ phase (Fig. 5) [20]. Here, as the absorbance of trans chains, the band at 840 cm^{-1} is contributed by both β and γ phases. In this case, the γ phase can be firstly excluded by the absences of the 812 and 1234 cm^{-1} absorptions. Based on this observation, together with the above XRD result indicating no related diffraction peak, the γ form can be removed. For neat PVDF, the appearance of 615, 764, 796 and 976 cm^{-1} which are indicative of α phase, suggesting the sample was α-form dominated (curve S1). With the addition of the MWCNTs, the intensity at 840 cm^{-1} become stronger, while the bands (including 615, 764, 796 and 976 cm^{-1}) indicative of

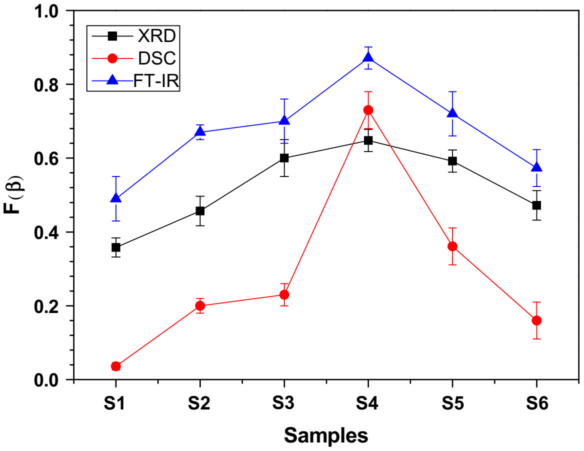

Fig. 6. The β-phase content derived from XRD, DSC and FT-IR measurements (a) and the comparison of the β-phase content, $F(\beta)$, from some recent publications.

Table 2
The comparison of the β-phase content, $F(\beta)$, from some recent publications.

Methods	a	b	c	d	e	f	g	h	i	j
$F(\beta)$ (%)	54.0	74.5	75.0	76.1	80.0	85.0	86.1	86.5	87.0	97.0

a. PVDF samples obtained from homogeneous phase reactions in supercritical CO_2 [36].
b. PVDF/nanosilica composites were prepared by solution blending [32].
c. PVDF fibers prepared by electrospinning from DMF solutions [20].
d. PVDF/MWCNTs composites prepared by solution blending [43].
e. PVDF films prepared through changing the drying temperature in the two different solution [38].
f. PVDF (Kynar films) treated by stretching procedure [39].
g. Commercial β-PVDF films immersed in eight different reagents for different exposure times [40].
h. PVDF films produced *via* film blowing extrusion [41].
i. Our PVDF/MWCNTs-modified by HBCs films prepared by solution coagulation.
j. Nylon-6/PVDF blends prepared by melt-blending under stretching [42].

α-crystal form become weaker, implying that α-phase is gradually replaced by β-phase. Similar observation had previously reported in this group [32]. Surprisingly, when the HBCs–assisted MWCNTs (HBCs–CNTs) are incorporated, all α-phase-related bands are weakened profoundly, replaced by the evidently enhanced 840 cm^{-1} band. As noted, although the loadings of HBCs are all the same for samples, ca.0.3% (mass fraction) for S3–S6, different types of HBCs–CNTs show a difference in the improvement of the β-phase content of PVDF. From the FT-IR results, the content of β phase $F_3(\beta)$ can be calculated by following equation [13,37], i.e.

$$F_3(\beta) = \frac{A_\beta}{1.26A_\alpha + A_\beta} \tag{3}$$

where A_α, A_β are the integral area of bands at 763 (α phase) and 840 cm^{-1} (β phase), respectively.

The conclusive comparison concerning the $F(\beta)$ values from different techniques, including XRD, DSC and FT-IR measurements is displayed in Fig. 6. As we mentioned above, three set of data present the same tendency and all β-phase increase noticeably upon the addition of HBCs modified MWCNTs. For S4, specifically, the hybrid has the highest $F(\beta)$ values. In order to comparatively show our success, we intentionally give some results of $F(\beta)$ values,

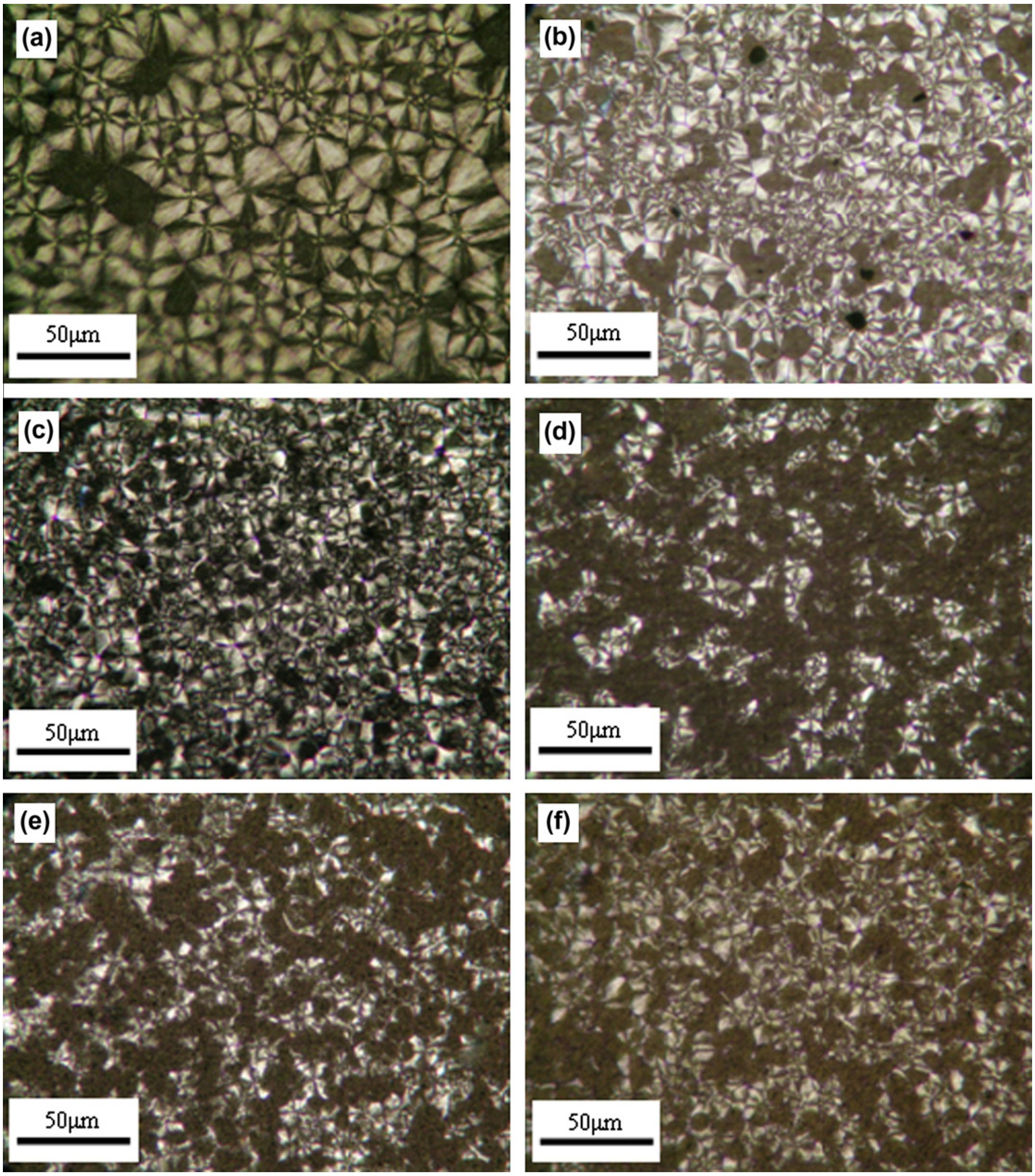

Fig. 7. Polarized optical microscopy images of the pure PVDF (S1, a), hybrid films S2 (b), S3 (c), S4 (d), S5 (e) and S6 (f).

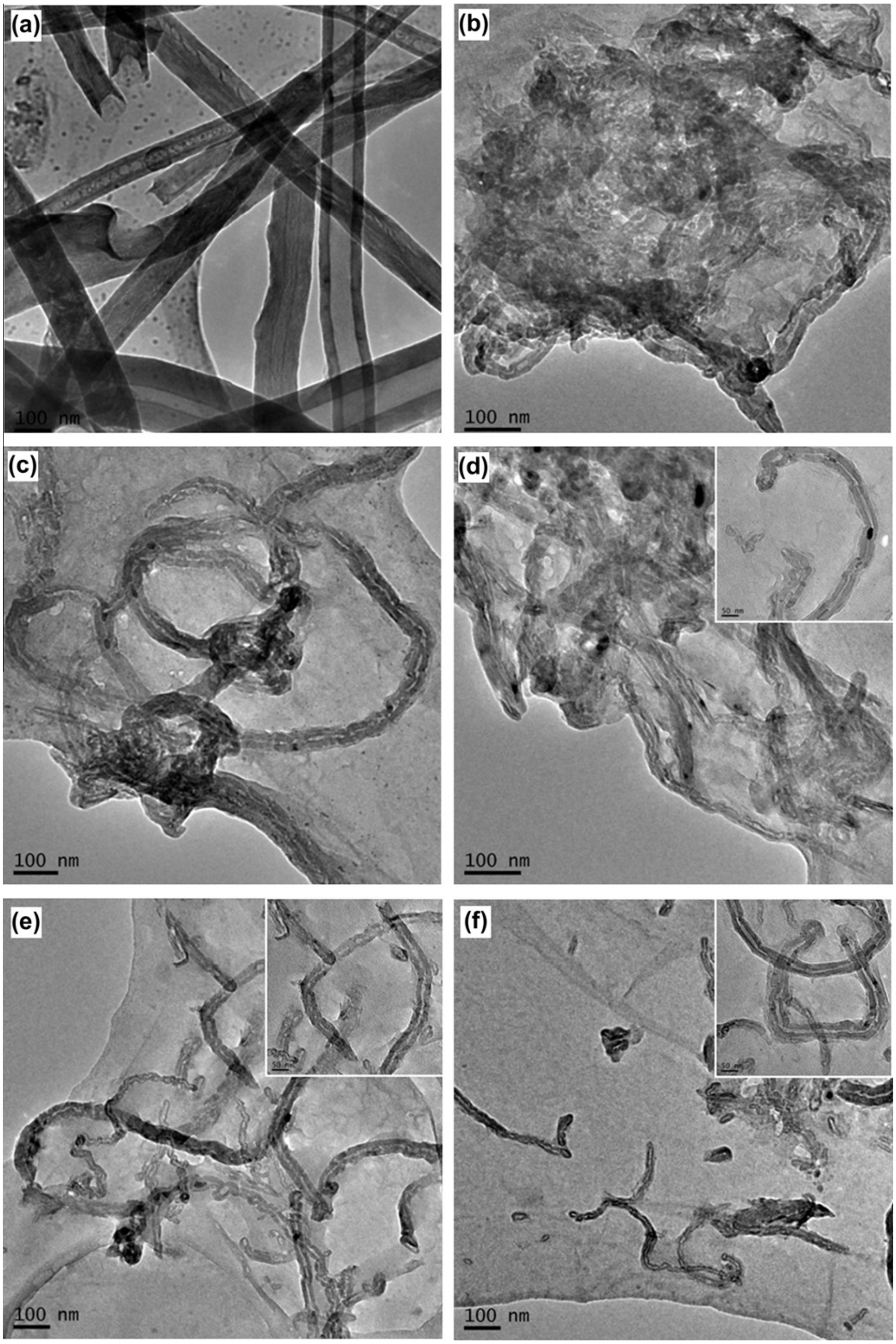

Fig. 8. TEM images of the purified MWCNTs (a), hybrid films S2 (b), S3 (c), S4 (d), S5 (e) and S6 (f). The insets in (d), (e), (f) are the high-resolution of TEM images showing the morphologies of MWCNTs in the PVDF matrix.

which were collected from recent publications (Table 2). As clearly seen, the $F(\beta)$ obtained by our protocol is comparable or better than others considering the fact that the exceptional high $F(\beta)$ value (ca. 95%,) was obtained in the polymer blend of Nylon-6 and PVDF, rather than the neat PVDF [34]. As matter of fact, MWCNTs had a positive effect on the increase of the β-phase crystalline forms of PVDF, while the agglomeration from the MWCNTs is still a serious concern [24]. Hence, we believe that the substantive improvement in $F(\beta)$ of PVDF should be originated from the strong dispersive effect from the HBCs. In this case, the chemical composition and the special structure will endow the HCPs with the amphiphilic-like property of surfactant in the dispersion of CNTs in the PVDF matrix [27]. Accordingly, then, how the HCPs affect the beta phase formation is understandable. Take the S4 as the example, in which the HBC-2 was used as the dispersing agent. Comparing other 2 HCPs employed, the HBC-2 has highest molecular weight (M_w = 35.1 kD) and highest content of p-chloromethyl styrene (70 mol.%) (see Table 1), and accordingly has the highest concentration of polar chloro-group. Therefore, we believed that, the enhanced electrostatic force between the HCPs (chloro-group, mainly) and PVDF host (F atoms) will result in the improved beta phase content to [35].

Polarized optical microscopy (POM) images in Fig. 7 shows vividly the morphologies of isothermally crystallized samples of neat PVDF (S1, Fig. 7a), MWCNTs-added PVDF (S2, Fig. 7b) and PVDF hybrids with different HBCs–wrapped MWCNTs (S3–S6, Figs. 7c and 6f). As indicated, the spherulitic size decreases with the addition of MWCNTs, and this observation become particularly evident with the introduction of HBCs–wrapped MWCNTs. Obviously, HBCs–wrapped MWCNTs indicate a higher nucleating ability than the naked MWCNTs. Further, the smaller and highly packed spherulite also implies the homogenous distribution of HBCs–wrapped MWCNTs. This aspect is also consistent with the SEM results of the samples (see Fig. S2 in Supplementary information). In addition, the relatively uniform and homogeneous features of the hybrids films can be seen in Fig. S3.

Moreover, the effect of HBCs on the dispersion of MWCNTs is assessed directly *via* TEM and the results are given in Fig. 8. Compared with the naked MWCNTs in the PVDF (Fig. 8b), the MWCNTs wrapped by varied HBCs, without obvious aggregation or preferred alignment, are more homogenously and randomly dispersed in PVDF matrix (Fig. 8c–f). Upon close checking, most of MWCNTs remain curved or even interwoven throughout the PVDF matrix, indicating their extreme flexibility [43]. Moreover, the entangling degree is tremendously reduced, with a large percentage of individual nanotubes being present. Comparing the TEM images of purified MWCNTs (Fig. 8a), direct evidence for the presence of PVDF molecules on the MWCNTs surface can be found in the hybrid films (Fig. 8c–f); i.e. the purified MWCNTs surfaces are very smooth and demonstrate clear edges, while the MWCNTs surfaces of the hybrids are covered by a polymeric layer, which results from the adsorption of segment of PVDF by the nonspecific molecular interactions between the C–H groups of PVDF and MWCNTs [44,45]. This interaction would be inevitably favorable for the formation of the all-trans β phase, possessing the polymer chains stacked with their respective polarizations aligned in the same direction.

4. Conclusions

In summary, we have demonstrated that the crystal distribution in PVDF could be alternated significantly by the addition of trace of MWCNTs wrapped by hyperbranched copolymers. By using combined measurements, we obtained a highly consensus in regarding to the ratio of crystal phases in PVDF, i.e. the β-phase can be enhanced remarkably with the HBCs–wrapped MWCNTs. As described, this presented procedure has the advantages of facile, fast and efficient to obtain the β-phase content which comparable or higher than otherwise reports. As far as we know, this is the first case that the HBCs are used to enhance the crystal distribution in PVDF.

Since the filler uses in this case is MWCNTs, which is in nano scale, thus the success in tuning the phase distribution can be attributed to the good dispersion being rendered by the highly branched three-dimensional globular architecture created by the HBCs. Therefore, the method described herein offers a unique possibility to prepare uniform, robust and thermal stable thin films with enhanced β-phase and this result will accordingly influence the electroactive response of the materials [46].

Acknowledgments

This work was supported by the National Foundation of Nature Science (21072221), President Fund of Graduate University of CAS (095101CY00), and Grant KF2008-04 from the State Key Laboratory of Environmental Chemistry and Ecotoxicology, Research Center for Eco-Environmental Sciences, Chinese Academy of Sciences.

Appendix A. Supplementary material

Supplementary data associated with this article can be found, in the online version, at doi:10.1016/j.jcis.2011.07.042.

References

[1] A.J. Lovinger, Science 220 (1983) 1115–1117.
[2] W.Z. Ma, J. Zhang, S.J. Chen, X.L. Wang, J. Macromol. Sci. Part B: Phys. 47 (2008) 434–442.
[3] W.Z. Ma, J. Zhang, X.L. Wang, J. Mater. Sci. 43 (2008) 398–406.
[4] R. Gregorio, J. Appl. Polym. Sci. 100 (2006) 3272–3279.
[5] J.B. Lando, H.G. Olf, J. Polym. Sci. Part A: Polym. Chem. 4 (1966) 941–948.
[6] K.P. Pramoda, A. Mohamed, I.Y. Phang, T.X. Liu, Polym. Int. 54 (2005) 226–236.
[7] D. Shah, P. Maiti, E. Gunn, D.F. Schmidt, D.D. Jiang, C.A. Batt, ER. Giannelis, Adv. Mater. 16 (2004) 1173–1177.
[8] T.U. Patro, M.V. Mhalgi, D.V. Khakhar, A. Misra, Polymer 49 (2008) 3486–3492.
[9] S. Ramasundaram, S. Yoon, K.J. Kim, C. Park, J. Polym. Sci. Part B: Polym. Phys. 46 (2008) 2173–2181.
[10] L. Yu, P. Cebe, Polymer 50 (2009) 2133–2138.
[11] L. Priya, J. Jog, J. Polym. Sci., B: Polym. Phys. 40 (2002) 1682–1687.
[12] K. Tenneti, Y. Li, F. Ko, I. Sics, B. Hsiao, D. Dillon, Polymer 47 (2006) 1678–1685.
[13] P. Cebe, D. Cherdack, J. Crawford, B. Ince, M. Jenkins, J. Pan, M. Reveley, N. Washington, N. Wolchover, J. Buckley, Polymer 47 (2006) 2411–2417.
[14] L. He, Q. Xu, C. Hua, R. Song, Polym. Compos. 31 (2010) 921–927.
[15] S. Huang, W.A. Yee, W.C. Tjiu, Y. Liu, M. Kotaki, Y.C. Boey, J. Ma, T.X. Liu, X.H. Lu, Langmuir 24 (2008) 13621–13626.
[16] J. Andrew, J. Mack, D. Clarke, Mater. Res. 23 (2008) 105–110.
[17] J. Andrew, D. Clarke, Langmuir 24 (2008) 8435–8439.
[18] P. Martins, C.M. Costa, S. Lanceros-Mendez, Physica A 103 (2011) 233–237.
[19] R. Zheng, A. He, J. Li, C.C. Han, Macromol. Rapid Commun. 28 (2007) 2159–2164.
[20] J.S. Andrew, D.R. Clarke, Langmuir 24 (2008) 670–673.
[21] W.A. Yee, A.C. Nguyen, P.S. Lee, M. Kotaki, Y. Liu, B.T. Tan, S. Mhaisalkar, X.H. Lu, Polymer 49 (2008) 4196–4203.
[22] A. Takeno, N. Okui, T. Kitoh, M. Muraoka, S. Umemoto, T. Sakai, Thin Solid Films 202 (1991) 205–211.
[23] A.C. Rastogi, S.B. Desu, Vapor Depos. 12 (2006) 742–749.
[24] J. Sakata, M. Mochizuki, Thin Solid Films 195 (1991) 175–182.
[25] L. He, K. Yao, Appl. Phys. Lett. 89 (2006) 112909–112912.
[26] S. Yoon, A.A. Prabu, K.J. Kim, C. Park, Macromol. Rapid Commun. 29 (2008) 1316–1329.
[27] L. Yao, W.Y. Yang, J. Yang, L.H. He, J. Sun, R. Song, Z. Ma, W. Huang, Nanoscale 3 (2011) 916–918.
[28] Z.W. Zhang, Q. Xu, Z.M. Chen, J. Yue, Macromolecules 41 (2008) 2868–2873.
[29] C.H. Zhang, J.G. Li, J. Zhang, L.Y. Zhang, H.Y. Li, Polym. Adv. Technol., 2009. doi:10.1002/pat.1491.
[30] J.K. Yuan, Z.M. Dang, S.H. Yao, J.W. Zha, T. Zhou, S.T. Li, J.B. Bai, J. Mater. Chem. 20 (2010) 2441–2447.
[31] M. Imran-ul-hap, B. Tiersch, S. Beuermann, Macromolecules 41 (2008) 7453–7462.
[32] R. Song, D.B. Yang, L.H. He, J. Mater. Sci. 42 (2007) 8408–8415.
[33] T. Umasankar Patro, M.V. Mhalgi, D.V. Khakhar, A. Misra, Polymer 49 (2008) 3486–3499.
[34] E.G. Noya, D. Srivastava, L.A. Chernozatonskii, M. Menon, Phys. Rev. B 70 (2004) 115416.
[35] T. Zhou, J. Zha, R. Cui, B. Fan, J. Yuan, Z. Dang, ACS Appl. Mater. Interfaces, 2011. doi:org/10.1021/am200492q.
[36] C.W. Nan, G. Liu, Y.H. Lin, M. Li, Appl. Phys. Lett. 85 (2004) 3549–3551.
[37] Y.S. Song, J.R. Youn, Carbon 43 (2005) 1378–1385.
[38] A. Salimi, A. Yousefi, J. Poly. Sci. Part B: Polym. Phys. 42 (2004) 3487–3494.
[39] W. Yang, T.H. Fang, S.Y. Liu, Y.C. Lin, Mater. Sci. Eng., A 480 (2008) 477–487.
[40] M.P. Silva, G. Botelho, J.G. Rocha, S. Lanceros-Mendez, Polym. Test. 29 (2010) 613–619.
[41] B. Mohammadi, A.A. Yousefi, S.M. Bellah, Polym. Test. 26 (2007) 42–51.
[42] B. Na, W. Xu, R. Lv, Z. Li, N. Tian, S. Zou, Macromolecules 43 (2010) 3911–3916.
[43] M. Nasir, H. Matsumoto, T. Danno, M. Minagawa, T. Irisawa, M. Shioya, A. Tanioka, J. Polym. Sci. Part B: Polym. Phys. 44 (2006) 779–787.
[44] L.H. He, X.L. Zheng, Q. Xun, J. Phys. Chem. B 114 (2010) 5257–5262.
[45] D. Baskaran, J.W. Mays, M.S. Bratcher, Chem. Mater. 17 (2005) 3389–3397.
[46] J. Gomes, J.S. Nunes, S. Lanceros-Mendez, Smart Meter. Struct. 19 (2010) 065010.